Vector Hysteresis Modeling in Arbitrarily Shaped Objects Using an Energy Minimization Approach

Amr A. Adly [1] and Salwa K. Abd-El-Hafiz [2]

[1] Electrical Power and Machines Department
[2] Engineering Mathematics and Physics Department
Faculty of Engineering, Cairo University, Giza 12613, Egypt
amradly@ieee.org, salwa@computer.org

Abstract ─ It is known that proper and efficient modeling of vector hysteresis is crucial to the precise design and performance estimation of electric power devices and magnetic recording processes. Recently, discrete Hopfield neural networks have been successfully utilized in the construction of vector hysteresis models. This paper presents a novel energy-minimization Hopfield neural network approach to implement Stoner-Wohlfarth-like vector hysteresis operators in triangular sub-regions. Advantages of the approach stem from the non-rectangular nature of such operators, which could mimic major hysteresis loops as well as their implementation in the most commonly used triangular discretization sub-domains. Details of the approach are given in the paper.

Index Terms ─ Discrete Hopfield neural network, energy minimization, shape anisotropy, vector Hysteresis.

I. INTRODUCTION

Electromagnetic field computation in nonlinear media and media exhibiting hysteresis is, in general, a crucial activity to a wide variety of applications such as those involving analysis of magnetic recording processes and determination of core losses in power devices (see, for instance, [1-4]). In this context, only computationally efficient vector hysteresis models may be practically utilized in numerical field computation methodologies, which are indispensable for handling complicated device geometries and excitation schemes.

In the past, substantial efforts focusing on the efficiency enhancement of typical vector hysteresis models have been reported (refer, for instance, to [5]). The notion of implementing an arbitrary elementary hysteresis operator using a dual-node discrete Hopfield neural network (HNN) having positive feedback values was first introduced in [6]. In this approach, switching thresholds of the operator were easily manipulated through the feedback factor as well as an input offset term. Later on, discrete HNNs have been successfully configured to construct scalar – as well as coupled pairs of – hysteresis operators [7-9]. Moreover, an enhancement of the aforementioned HNN configuration was carried out in [10] for the implementation of Stoner-Wohlfarth-like operators. An important advantage of this enhancement stems from the non-rectangular nature of the generated operators which minimizes the number of operators required to mimic a specific loop.

This paper presents an energy minimization HNN approach to model vector hysteresis in triangular sub-regions. More specifically, the approach further generalizes the work in [10] by correlating a triangular geometrical configuration to the coupling coefficients of a corresponding 3-node HNN. Using this approach, it is possible to account for shape anisotropy implications on vector hysteresis. The approach could also be utilized in field computation in media exhibiting hysteresis.

II. REALIZATION OF A TRIANGULAR SUB-REGION INVOLVING MEDIA EXHIBITING HYSTERESIS

The proposed 2D methodology is based on the utilization of the hybrid discrete-continuous activation function proposed in [10] in a 3-node HNN with positive feedbacks, as shown in Fig. 1. It should be pointed out that this configuration is genuinely proposed in this work to realize the primitive scalar and vector hysteresis properties for a triangular sub-region u having arbitrary geometry. Within this proposed configuration, the orientation of every node is assumed to be along the line joining the u^{th} triangle center point to its corresponding vertex. Positive feedbacks $k_{i,j}^{(u)}$ between different triangle nodes i and j are assumed to be given by:

$$k_{i,j}^{(u)} = k_{copl} \left| \cos(\varphi_{ij}^{(u)}) \right|, \tag{1}$$

where, k_{copl} is a pre-selected coupling factor ≤ 1 and $\phi_{ij}^{(u)}$ is the angle subtended between nodes i and j orientations as shown in Fig. 2.

Assuming a hybrid activation function $f(x)$ [10] given by:

Submitted On: June 6, 2015
Accepted On: May 21, 2016

$$f(x) = c\, f_c(x) + (1-c)\, f_d(x), \quad (2)$$

where, c is a positive constant ≤ 1 while $f_c(x)$ and $f_d(x)$ are the sigmoid continuous and signum discrete activation functions, respectively, given by:

$$f_c(x) = \tanh(ax), \quad a > 0, \quad (3)$$

$$f_d(x) = \begin{cases} +1 & \text{if } x > 0 \\ -1 & \text{if } x < 0 \\ \text{unchanged} & \text{if } x = 0 \end{cases}. \quad (4)$$

The new hybrid activation rule for, say, node *i* thus becomes:

$$m_i^{(u)}(t+1) = c\, f_c(net_i^{(u)}(t)) + (1-c)\, f_d(net_i^{(u)}(t)), \quad (5)$$

where $m_i^{(u)}$ is the node output while $net_i^{(u)}$ maybe defined, in accordance with (1) and Fig. 1, by:

$$net_i^{(u)}(t) = \bar{h}^{(u)}(t) \bullet \left(\frac{\bar{m}_i^{(u)}}{m_i^{(u)}} \right) + \sum_{j=1, j\neq i}^{3} k_{i,j}^{(u)} m_j^{(u)}(t), \quad (6)$$

where $\bar{h}^{(u)}$ is the external input applied to the u^{th} triangle.

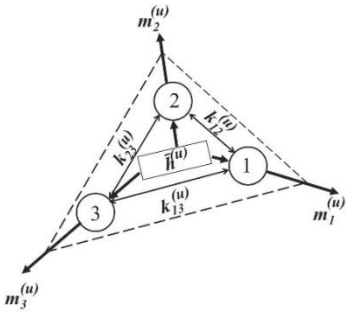

Fig. 1. Realization of a basic vector hysteresis operator representing a triangular sub-region using a tri-node HNN.

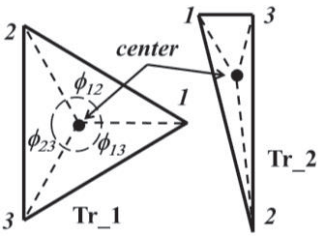

Fig. 2. Examples of two triangular sub-regions having different aspect ratios.

The state of this network converges to the minimum of the following energy function:

$$E^{(u)} = -\sum_{i=1}^{3} \left\{ \bar{h}^{(u)} \bullet \bar{m}_i^{(u)} + \frac{1}{2} \sum_{j=1, j\neq i}^{3} k_{i,j}^{(u)} m_i^{(u)} m_j^{(u)} \right\}. \quad (7)$$

For every applied external input $\bar{h}^{(u)}$, well established HNN time-stepping algorithms are utilized in accordance with (5)-(7) to achieve a minimum value for the u^{th} triangle energy $E^{(u)}$ (see, for instance, [11, 12]). From the superposition principle, overall triangle output $\bar{m}^{(u)}$ may be computed from:

$$\bar{m}^{(u)} = \sum_{i=1}^{3} \bar{m}_i^{(u)}. \quad (8)$$

In order to demonstrate the effect of the geometrical configuration on a triangle's primitive scalar and vector hysteresis properties, consider the 3 triangles whose geometrical details are given in Fig. 3 and Table 1. x-axis scalar and rotational *M-H* curves corresponding to the three triangles under consideration are shown in Figs. 4 and 5, respectively.

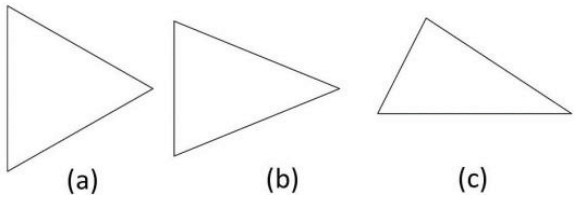

Fig. 3. Three arbitrary chosen triangles having different geometrical configurations: (a) Tr_1, (b) Tr_2, and (c) Tr_3.

Table 1: Geometrical details of the triangles shown in Fig. 3

Triangle	Orientation of the Lines Joining Center Point and Vertices
Tr_1	0°, +120°, -120°
Tr_2	0°, +135°, -135°
Tr_3	-15.94°, +116.56°, -158.2°

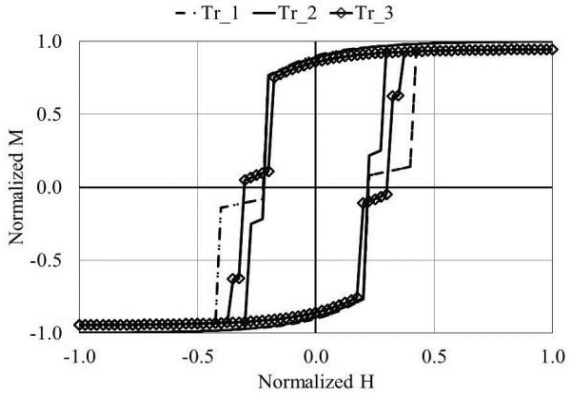

Fig. 4. Normalized scalar *M-H* curves along the x-axis corresponding to the three triangles shown in Fig. 3 for $k_{copl} = 0.3$, $a = 3$ and $c = 0.7$.

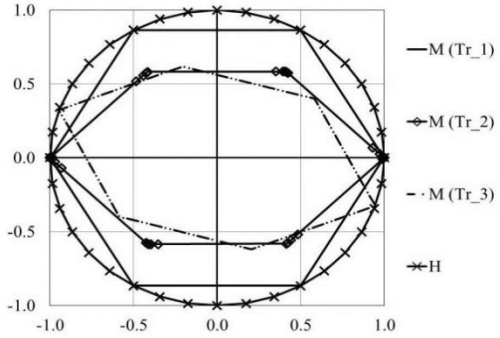

Fig. 5. Normalized rotational *M-H* curves corresponding to the three triangles shown in Fig. 3 for $k_{copl}=0.3$, $a=3$ and $c=0.7$.

Few important observations, which are in full harmony with magnetism physical principles, may be drawn from these figures [13]. For instance, Fig. 4 suggests that the triangle having the least stretch towards the x-axis (i.e., Tr_1) is the one having the widest (hardest) scalar x-axis *M-H* curve. Moreover, for the triangle which does not have a vertex orientation along the x-axis (i.e., Tr_3) it is not easy to achieve full saturation. Furthermore, Fig. 5 clearly demonstrates the tri-axis anisotropy associated with a triangular sub-region. In addition, the impact of the geometrical configuration on the rotational *M-H* curves symmetry as well as tilting is clearly demonstrated in Fig. 5.

More importantly, the ability of the proposed approach to realize different *M-H* curve width and squareness for a particular triangle is clearly demonstrated in Figs. 6 and 7. In these two figures, different scalar *M-H* curves are generated for triangle Tr_1 by varying k_{copl} and c, respectively. Likewise, it could be demonstrated that the scalar *M-H* curves may be modified by varying a. This fact highlights the ability of the approach to custom fit specific hysteresis curves.

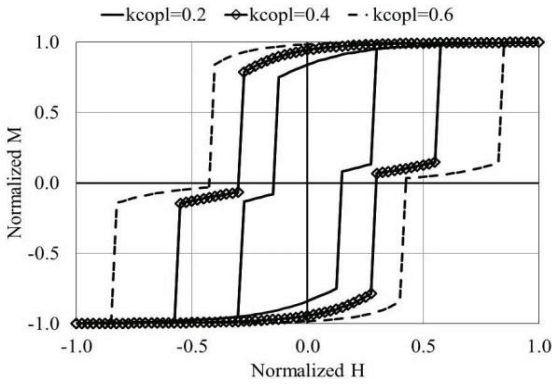

Fig. 6. Normalized scalar *M-H* curves along the x-axis corresponding to the triangle Tr_1 for $a=3$, $c=0.7$ and $k_{copl}=0.2, 0.4, 0.6$.

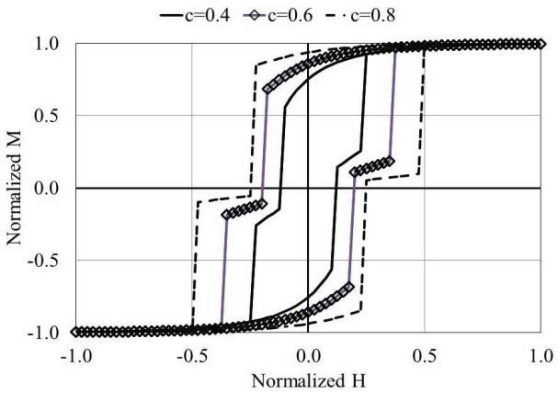

Fig. 7. Normalized scalar *M-H* curves along the x-axis corresponding to the triangle Tr_1 for $k_{copl}=0.3$, $a=3$ and $c=0.4, 0.6, 0.8$.

III. VECTOR HYSTERESIS MODELING FOR ARBITRARILY SHAPED OBJECTS

As previously stated, any two-dimensional geometrical arbitrary shape may be approximated by an ensemble of triangular sub-regions. Obviously, no shape anisotropy is introduced for circular configurations. In order to demonstrate the applicability of the proposed approach, the circular geometrical configuration shown in Fig. 8 (a) is considered to fit experimentally measured hysteresis loop of an isotropic magnetic sample. More specifically, this circular configuration is assumed to be composed of an ensemble of 36 triangular sub-regions. Identification of the model is achieved through the determination of unknowns k_{copl}, c and a that result in best fit with the experimental data.

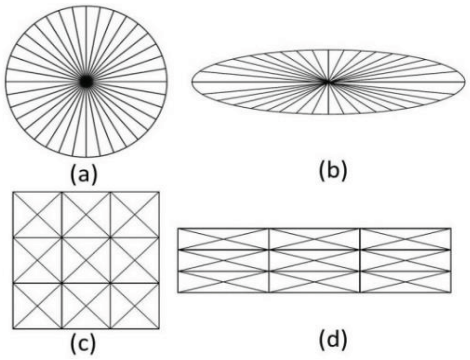

Fig. 8. Four geometrical configurations each comprising 36 triangular sub-regions and corresponding to: (a) a circle, (b) an ellipse, (c) a square, and (d) a rectangle.

For the case under consideration, the method of least square errors was utilized to carry out this process. As a result, values $k_{copl}=0.38$, $a=1.2$ and $c=0.3$ were found to give the best possible qualitative and quantitative

fit for the experimentally measured loop as shown in Fig. 9. Rotational *M-H* curves of the overall ensemble demonstrating the expected isotropic nature is also shown in Fig. 10 (a). Moreover, a comparison between measured and computed M rotational component phase lag corresponding to different rotating H amplitudes is shown in Fig. 10 (b). This figure demonstrates the good qualitative and quantitative values achieved while using an extremely low number of hysteresis operators.

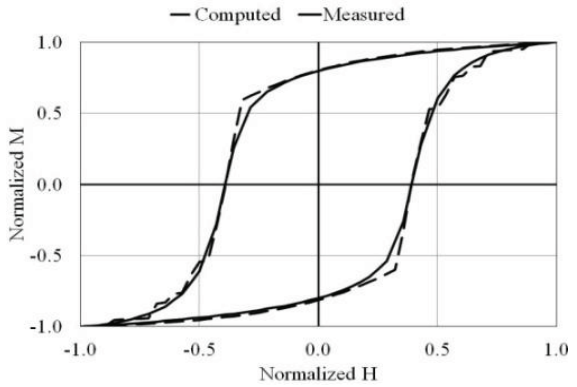

Fig. 9. Comparison between measured and computed hysteresis loop for the 36 triangular sub-region geometrical configuration shown in Fig. 8 (a) corresponding to $k_{copl}=0.38$, $a=1.2$ and $c=0.3$.

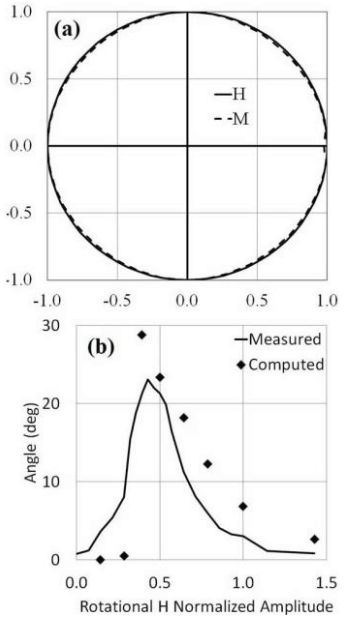

Fig. 10. (a) Rotational *M-H* curves for the geometrical configuration shown in Fig. 8 (a) and corresponding to $k_{copl}=0.38$, $a=1.2$ and $c=0.3$, and (b) phase lag of M rotational components for different rotational H amplitudes.

In order to demonstrate the proposed approach ability to account for scalar and vector hysteresis properties variations as a result of introduced shape anisotropy, three additional geometrical configurations were considered. In specific, a square as well as a rectangle and an ellipse both having an aspect ratio of 4 were considered as shown in Figs. 8 (b)-(d).

For consistency purposes, each of these geometrical configurations was assumed to be comprised of 36 triangular sub-regions and to have the same overall unity area. Results given in Figs. 11-13 clearly suggest that the proposed approach could be successfully utilized in predicting overall hysteresis properties variations resulting from shape-introduced anisotropy. For instance, while the scalar hysteresis loop of a square object deviates from that of a circular object, loops along the *x*- and *y*-directions are identical. Nevertheless, square nature of the object may be easily inferred from its rotational *M-H* curve. On the other hand, the double aspect ratio assumed for each of the ellipsoidal and rectangular objects introduces an anisotropic behavior demonstrated by the clear deviation between generated scalar hysteresis loops along *x*- and *y*-directions. Scalar loops for the aforementioned two objects are not the same. This is also demonstrated by their different rotational *M-H* curves.

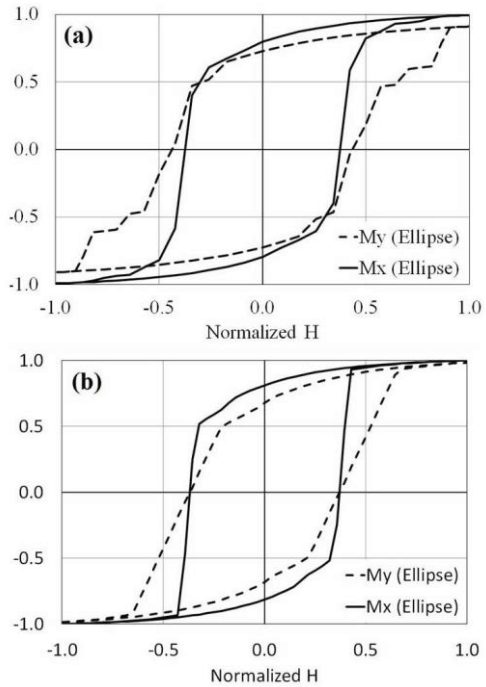

Fig. 11. Scalar *M-H* curves along the x- and y-axes corresponding to Fig. 8 (b) and computed using: (a) the proposed approach for $k_{copl}=0.38$, $a=1.2$ and $c=0.3$, and (b) using standard demagnetization factors.

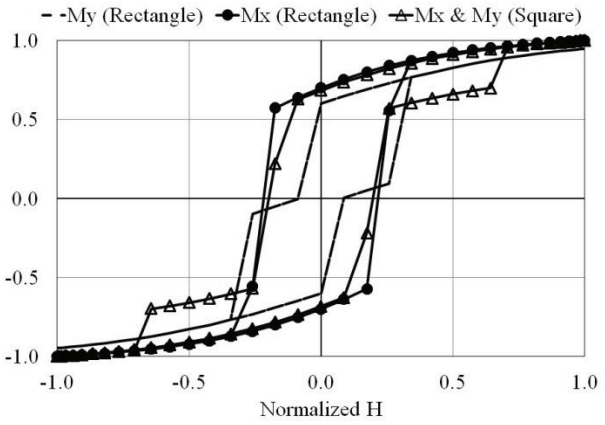

Fig. 12. Scalar *M-H* curves along the along the *x*- and *y*-axes corresponding to Figs. 8 (c)-(d) for $k_{copl} = 0.38$, $a = 1.2$ and $c = 0.3$.

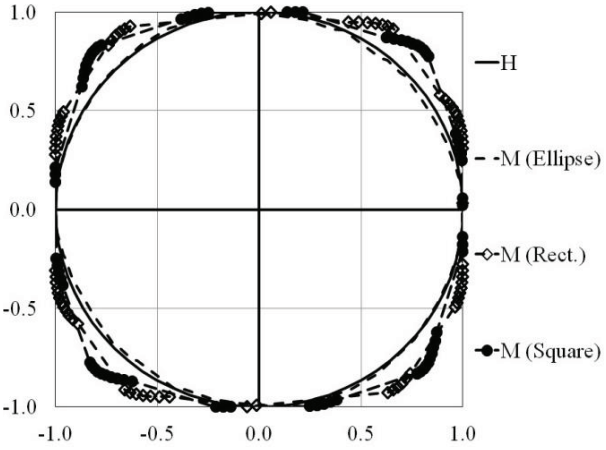

Fig. 13. Rotational *M-H* curves corresponding to Figs. 8 (b)-(d) for $k_{copl} = 0.38$, $a = 1.2$ and $c = 0.3$.

For a closer look at the total magnetization orientation for every triangular sub-region in each of the four geometrical configurations, please refer to Fig. 14. In this figure a snapshot of the above-mentioned magnetization magnitudes and orientations is shown for the instant when the applied field is maximum along the positive *x*-axis direction. Results given in this figure provide a somewhat detailed view of how individual triangular sub-region magnetizations tend to orient in the direction of the applied field. Those results are especially important as they demonstrate that local hysteresis losses may be accounted for and – by incorporating inter-domain interactions – could be extended for field computation purposes in media exhibiting hysteresis.

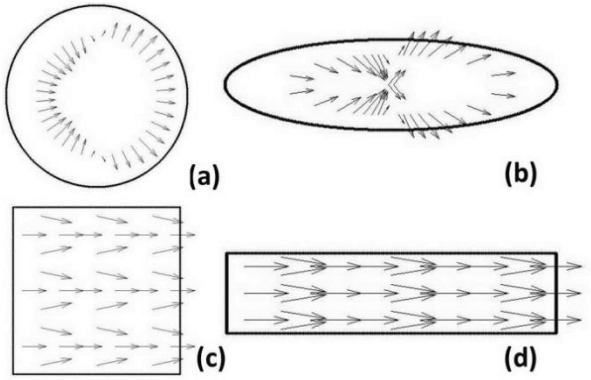

Fig. 14. Local magnetization magnitudes and orientations – on the triangular sub-region scale – corresponding to peak *x*-axis applied field for the regions shown in Fig. 8.

IV. CONCLUSIONS

It can be concluded from the previous analysis, discussion and results that a tunable efficient approach to mimic scalar and vector hysteresis properties in triangular sub-regions has been proposed. Using an ensemble of triangular sub-regions, it is demonstrated that the proposed approach may be successfully utilized in matching hysteresis properties of symmetrical bodies. It has also been shown that the proposed approach may be utilized to infer shape-anisotropy-introduced hysteresis properties variations. Given that the proposed approach may be utilized to determine the magnetization magnitude and orientation on the local triangular sub-region scale, it may be extended in the future for field computation applications in media exhibiting hysteresis.

REFERENCES

[1] A. A. Adly and S. K. Abd-El-Hafiz, "Utilizing particle swarm optimization in the field computation of non-linear magnetic media," *Journal of the Applied Computational Electromagnetics Society*, vol. 18, no. 3, pp. 202-209, 2003.

[2] A. Jacobus, "Nonlinear 3D numerical field calculation of a magnetic recording head," *IEEE Trans. Magn.*, vol. 24, no. 1, pp. 548-551, 1988.

[3] G. Friedman and I. D. Mayergoyz, "Computation of magnetic field in media with hysteresis," *IEEE Trans. Magn.*, vol. 25, no. 5, pp. 3934-3936, 1989.

[4] A. A. Adly, I. D. Mayergoyz, R. D. Gomez, and E. R. Burke, "Computation of fields in hysteretic media," *IEEE Trans. Magn.*, vol. 29, no. 6, pp. 2380-2382, 1993.

[5] E. Dlala, A. Belahcen, K. A. Fonteyn, and M. Belkasim, "Improving loss properties of the Mayergoyz vector hysteresis model," *IEEE Trans.*

Magn., vol. 46, no. 3, pp. 918-924, 2010.

[6] A. A. Adly and S. K. Abd-El-Hafiz, "Identification and testing of an efficient Hopfield neural network magnetostriction model," *Journal of Magnetism and Magnetic Materials*, vol. 263, no. 3, pp. 301-306, 2003.

[7] A. A. Adly and S. K. Abd-El-Hafiz, "Efficient implementation of vector Preisach-type models using orthogonally coupled hysteresis operators," *IEEE Trans. Magn.*, vol. 42, no. 5, pp. 1518-1525, 2006.

[8] A. A. Adly and S. K. Abd-El-Hafiz, "Efficient implementation of anisotropic vector Preisach-type models using coupled step functions," *IEEE Trans. Magn.*, vol. 43, no. 6, pp. 2962-2964, 2007.

[9] A. A. Adly and S. K. Abd-El-Hafiz, "Efficient vector hysteresis modeling using rotationally coupled step functions," *Physica-B: Condensed Matter*, vol. 407, no. 9, pp. 1350-1353, 2012.

[10] A. A. Adly and S. K. Abd-El-Hafiz, "Efficient modeling of vector hysteresis using a novel Hopfield neural network implementation of Stoner-Wohlfarth-like operators," *Elsevier Journal of Advanced Research*, vol. 4, no. 4, pp. 403-409, 2013.

[11] K. Mehrotra, C. K. Mohan, and S. Ranka, *Elements of Artificial Neural Networks*, MIT Press, Cambridge, MA, 1997.

[12] S. Haykin, *Neural Networks: A Comprehensive Foundation*, Prentice-Hall, Englewood Cliffs, NJ, 1999.

[13] R. M. Bozorth, *Ferromagnetism*, IEEE Press, New York, 1993.

Amr A. Adly received the B.S. and M.S. degrees in Electrical Power Engineering from Cairo University (CU) in 1984 and 1986, respectively, and the Ph.D. degree in Electrical Engineering from the University of Maryland (UM), College Park, USA, in 1992. He also worked as a Magnetic Measurement Instrumentation Senior Scientist at LDJ Electronics, Michigan, USA, during 1993-1994.

Since 1994, he has been a Faculty Member in the Faculty of Engineering, CU. He also worked in the US as a Visiting Research Prof. at UM, during the summers of 1996-2000. He worked in the period 2003-2004 as a Consultant to the UNESCO Cairo office and in 2006 as an Expert to the EU Commission. He also established and directed the R&D Administration at the Egyptian Industrial Modernization Center in the period 2006-2007. He served as the CU's Faculty of Engineering Vice Dean in the period 2010-2014. Since July 2014 he has been appointed as the Executive Director of the Science and Technology Development Fund (STDF).

Adly has published more than 120 reviewed papers and holds one U.S. patent. He also served for more than 10 years as a Member of the IEEE Magnetics Society Technical Committee. He reviewed more than 200 papers for international reputable journals, acted as the PI of several international research projects and supervised more than 15 Ph.D. and M.S. students. His research interests include electromagnetic field computation, magnetic materials, superconductivity, energy harvesting, magneto-hydro-dynamics, magnetic recording and power engineering.

Adly has been awarded the 1994 Egyptian State Encouragement Prize, the 2002 Shoman Foundation Young Arab Scientist Prize and the 2006 Egyptian State Excellence Prize. He has been promoted to IEEE Fellow status in 2011 and is currently serving in the Editorial Board of IEEE Transactions on Magnetics and Elsevier's Journal of Advanced Research.

Salwa K. Abd-El-Hafiz received the B.Sc. degree in Electronics and Communication Engineering from Cairo University, Egypt, in 1986 and the M.S. and Ph.D. degrees in Computer Science from the University of Maryland, College Park, Maryland, USA, in 1990 and 1994, respectively.

Since 1994, she has been working as a Faculty Member in the Engineering Mathematics and Physics Department, Faculty of Engineering, Cairo University, and has been promoted to a Full Professor in the same department in 2004. Since August 2014, she has also been working as the Director of the Technical Center for Career Development, Cairo University, Egypt. She co-authored one book, contributed one chapter to another book and published more than 60 refereed papers. Her research interests include software engineering, computational intelligence, numerical analysis, chaos theory and fractal geometry.

Abd-El-Hafiz is a recipient of the 2001 Egyptian State Encouragement Prize in Engineering Sciences, recipient of the 2012 National Publications Excellence Award from the Egyptian Ministry of Higher Education, recipient of the 2014 African Union Kwame Nkrumah Regional Scientific Award for Women in Basic Science, Technology and Innovation, recipient of several international publications awards from Cairo University and an IEEE Senior Member.